

Single-crystal silicon triple-torsional micro-oscillators for use in magnetic resonance force microscopy

Michelle D. Chabot^a, Troy C. Messina^a, Vladimir Mancevski^b, Casey W. Miller^a,
and John T. Markert^a

^aDepartment of Physics
University of Texas at Austin
Austin, Texas 78712

^bXidex Corporation
8906 Wall St., Suite 105
Austin, Texas 78754

ABSTRACT

Single-crystal silicon triple-torsional micro-oscillators have been fabricated, characterized, and modeled primarily for use in a magnetic resonance force microscope. These structures exploit a high-Q triple-torsional mode of oscillation while providing added stability. Fabrication involves lithography, reactive ion etch, and a final KOH wet-etch, with the final oscillator material being single-crystal boron-doped silicon. Typical oscillators were 250 nm thick and 10 – 200 microns in lateral dimensions. Finite element modeling provided the sequence and structure of the ten lowest-frequency modes and indicated that the upper torsional mode best isolates the motion from losses to the base. The oscillators were excited piezoelectrically and the resulting frequency-dependent motion was detected with fiber-optic interferometry, with a 0.002 nm/Hz^{1/2} resolution. Phase-sensitive motion detection at various points on the oscillator facilitated the assignment of the principle modes. Magnetic excitation was also investigated in order to best excite the torsional resonances. Cobalt micromagnets with moments below 10⁻¹² J/T were electron-beam deposited onto oscillators, and the magnetic forces were measured. MRFM, the primary intended application of these novel structures, is discussed; in particular, an overview is given of an experiment which uses a double-torsional micro-oscillator for the force detection of nuclear magnetic resonance. All topics discussed in this work are being combined in order to achieve a NMRFM single-sweep sensitivity as low as 10⁻¹⁶ N/Hz^{1/2} at room temperature.

Keywords: NMRFM, Micro-oscillators

1. INTRODUCTION

Advances in magnetic force microscopy have created a growing interest in fabricating and characterizing ultra-sensitive micro-mechanical oscillators. In particular, the field of magnetic resonance force microscopy¹⁻⁸ will benefit greatly from the fabrication of high-Q oscillators with low spring constants. However, due to the method used to invert the magnetization in nuclear magnetic resonance force microscopy (NMRFM), the resonant frequencies must be kept lower than approximately 50 kHz. A double-torsional micro-oscillator has been successfully used for the force detection of NMR, as will be discussed in Section 3.1. These double-torsional oscillators have been the focus of much research due to the high-Q characteristic of the upper torsional mode.⁹⁻¹¹ This work focuses on the related triple-torsional design for future use in a magnetic resonance force microscope. The geometry consists of a small, central moment of inertia, flanked symmetrically by larger moments which are connected to fixed mounts. These oscillators have been created using micro-electronic fabrication techniques. The characterization of these novel structures will be detailed in Section 2, and applicable experimental developments will be discussed in Section 3.

Send correspondence to markert@physics.utexas.edu

2. TRIPLE TORSIONAL OSCILLATORS

Fig. 1 shows the single-crystal silicon triple-torsional micro-oscillators which have been fabricated with thicknesses between 150 – 350 nm. The most significant difference between these oscillators and their double-torsional counterparts is that these are attached at both ends to a fixed base, whereas the double-torsionals are only attached at one end. This provides added stability while still allowing for the existence of the desired high-Q upper-torsional mode.

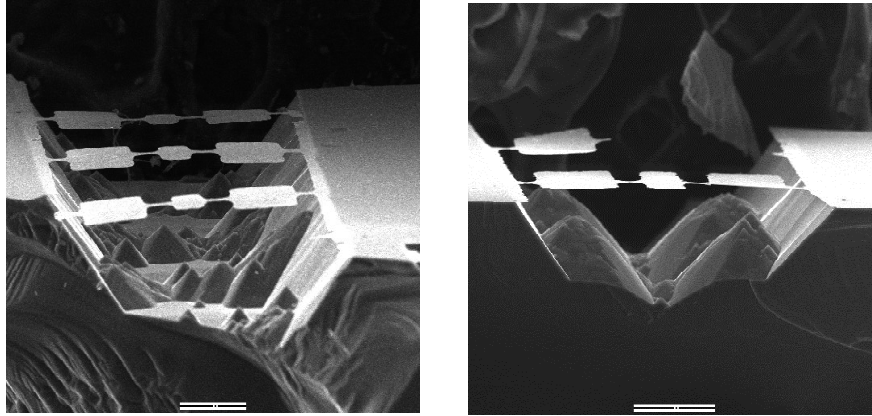


Figure 1. SEM showing successfully fabricated triple-torsional oscillators. (The broken oscillators are simply a result of cleaving the wafer into smaller parts after fabrication was complete.) The bar at the bottom of each is 100 μm .

The fabrication process¹¹ begins with single crystal silicon (100) wafers with a 750 nm film of oxide and a positive photoresist. The wafers are photo-exposed with the desired mask pattern. A reactive ion etch removes the oxide from the areas where the oscillators will be, leaving the rest of the wafer protected. Boron is then implanted into these exposed areas of silicon, and a post-implant anneal is done to re-crystallize the silicon. The remaining oxide is removed in a buffered oxide etch, and the wafers are then placed into a 10 percent solution of KOH. This anisotropic wet-etch removes the pure silicon while stopping on the highly boron-doped silicon.^{12–16} Once the oscillators are completely etched, they are freeze-dried in vacuum to eliminate the effects of stiction. At this point, the oscillators are ready for characterization.

The following section details the finite element modeling which was done to aid in the visualization of the lowest modes. Frequency scans have been performed using fiber-optic interferometry, and this is discussed in Section 2.2. Some terminology will be needed to discuss these structures: The large moments of inertia are referred to as the *wings*, the small central moment is the *head*, the fixed mounts are the *bases*, and the long thin pieces joining all of these are the *necks*.

2.1. Finite element modeling

Finite element modeling was done using ANSYS 5.6 software. The lateral dimensions used in modeling are given in Fig. 2; these were chosen as reasonable average values for the actual dimensions, to an accuracy of 10 μm . The thickness was assumed to be 200 nm, estimated from SEM images taken along the oscillator plane. Initially, the oscillators were modeled assuming that they were fixed where the necks meet the bases. The results for the lowest ten resonances indicated shapes much as would be expected. In particular, “bending”, “torsional”, “flapping”, and “lateral” modes were all observed. The thinness of the structure results in extreme curvature of the wings and head for both the bending and flapping modes. The wings and head in the torsional and lateral modes remain basically flat.

However, to more accurately model the actual oscillators, a base was included into the structure. This base consists of two parts, as indicated in Fig. 2. The part nearest the oscillator was made 50 μm long and 300 μm wide in order to account for the small over-hang which results from the final KOH wet-etch, and which is visible

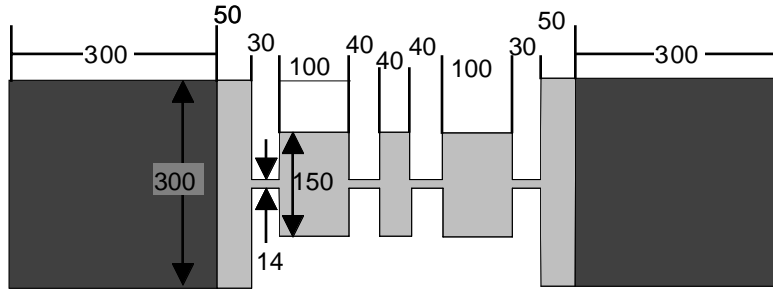


Figure 2. Dimensions used in the ANSYS finite element modeling of the triple torsional oscillators. Light gray indicates the areas which were chosen to have the properties of single crystal silicon and a thickness of 200 nm. Dark gray indicates the areas chosen to mimic the sturdiness of the fixed base.

in the SEM pictures of Fig. 1. This over-hang was made 200 nm thick single crystal silicon, exactly like the rest of the oscillator. The second part of the base (indicated by dark gray in Fig. 2) was modeled to account for the large thick silicon substrate. It was made five times thicker and five times stiffer (by changing the elastic modulus input) than the thin silicon structure. For this model, the two ends of the thick bases furthest from the oscillator were fixed in place.

Mode No.	Description	Frequency (kHz)
1	first bending	3.8
2	lower torsional	7.3
3	second bending	11.2
4	middle torsional	11.5
5	upper torsional	18.9
6	third bending	21.6
7	first base (see text)	29.9
8	second base (see text)	34.0
9	fourth bending	38.8
10	fifth bending	45.0

Table 1. A brief description of the first ten modes, along with their calculated frequencies.

Results for the first ten resonances are given in Fig. 3 and Fig. 4, with the resonance values given in Table 1.* As expected, the lowest mode is the fundamental bending mode. The second mode is the lowest torsional mode, in which all three moments rotate with the same phase. Mode 3 is the second bending mode, with some curvature (or “flapping”) in the wings. Mode 4 is the middle torsional resonance, in which the two wings move opposite to each other about a relatively fixed head. Of greatest interest is mode 5, the upper torsional mode, in which the two wings move together, opposite of the head. Most of the energy of oscillation for this mode is stored in the head, which is not directly coupled to the base. Thus damping due to energy dissipation to the base is minimized, and a high-Q is achieved. Mode 6 is the third bending mode, which, again, consists of significant curvature in the wings and head. Modes 7 and 8 are non-physical since both consist of an extreme displacement of the thick base. This is an artifact of the chosen specifications used in the model, and if a more realistic and

*If the thickness is changed, then the relative location of the resonances may also change. However, the shapes of the lowest modes will remain the same, regardless of exact order.

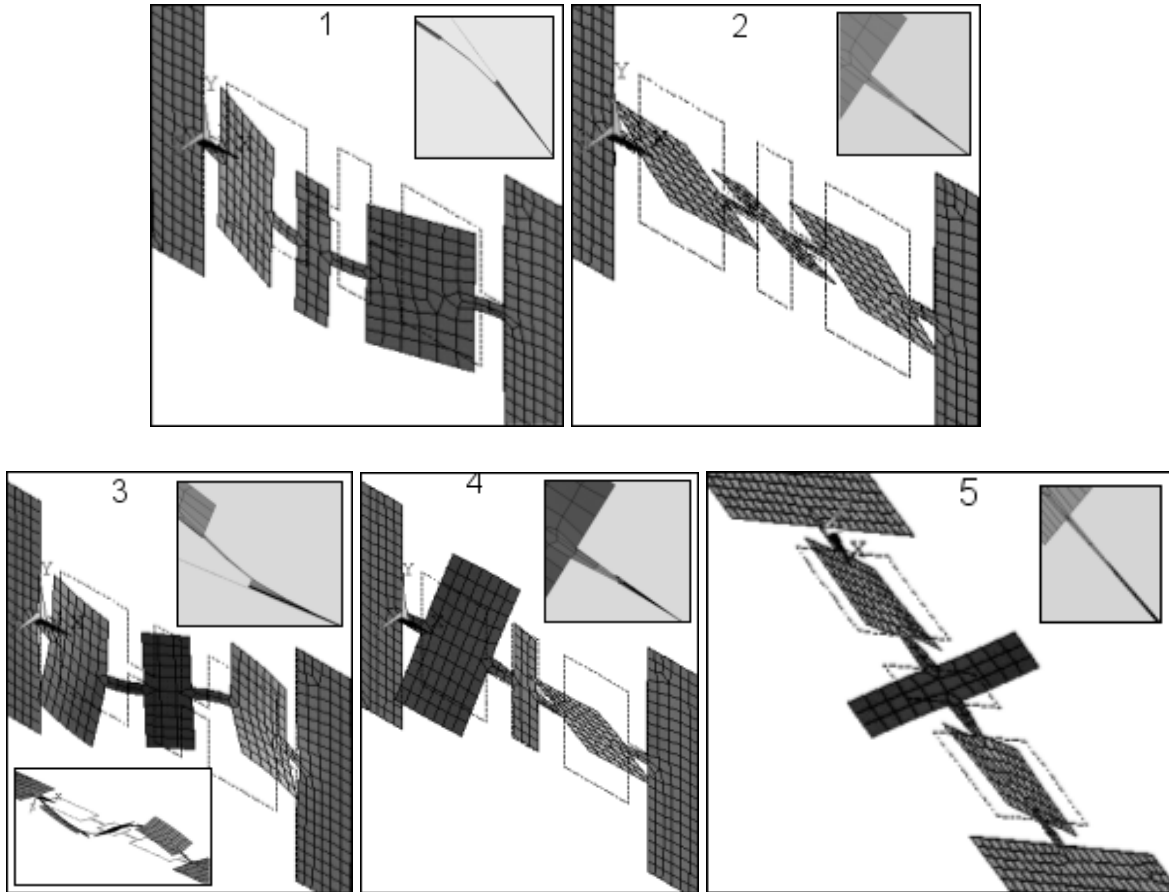


Figure 3. The lowest five modes of the triple torsional oscillator with the dimensions shown in Fig. 2. The upper right inset is a close-up view of where the wing is connected to the base via the neck. The thickness and the amount of bending in this area are a first indication of the amount of energy which is directly coupled to the base for each mode. Lower insets, if applicable, are side-views of each mode given for ease of visualization.

thicker base was modeled then these modes would not exist. For the first model in which the base was not considered, nothing resembling these two resonances was found in the lowest ten modes. Therefore these can be neglected, and Modes 9 and 10, the fourth and fifth bending modes, can be considered as the next physical resonances.

The upper right insets in Fig. 3 and Fig. 4 are a close-up view of where the wing is connected to the base via the neck. The thickness and the amount of bending in this area are a first indication of the amount of energy of oscillation which is directly coupled to the base for each mode. From this simple analysis, it can be seen that the bending modes result in a significant displacement of the base in the direction normal to the plane of the oscillator. Also, as the mode number increases, this displacement appears to increase, as can be seen in the insets of Modes 1, 3, 6, and 10. This indicates that the higher bending modes, which have much more curvature in the vicinity of the base, will most likely have more energy dissipation to the base and therefore more damping. On the other hand, the lowest torsional modes have the most movement near the base from the severe twisting of the neck. The upper torsional mode has the least twisting of the neck near the base and therefore is expected to have a higher Q .

These observations support initial intuition about the resonances of a triple torsional oscillator and the amount of direct energy coupling that each mode will have to the fixed bases. A detailed quantitative analysis

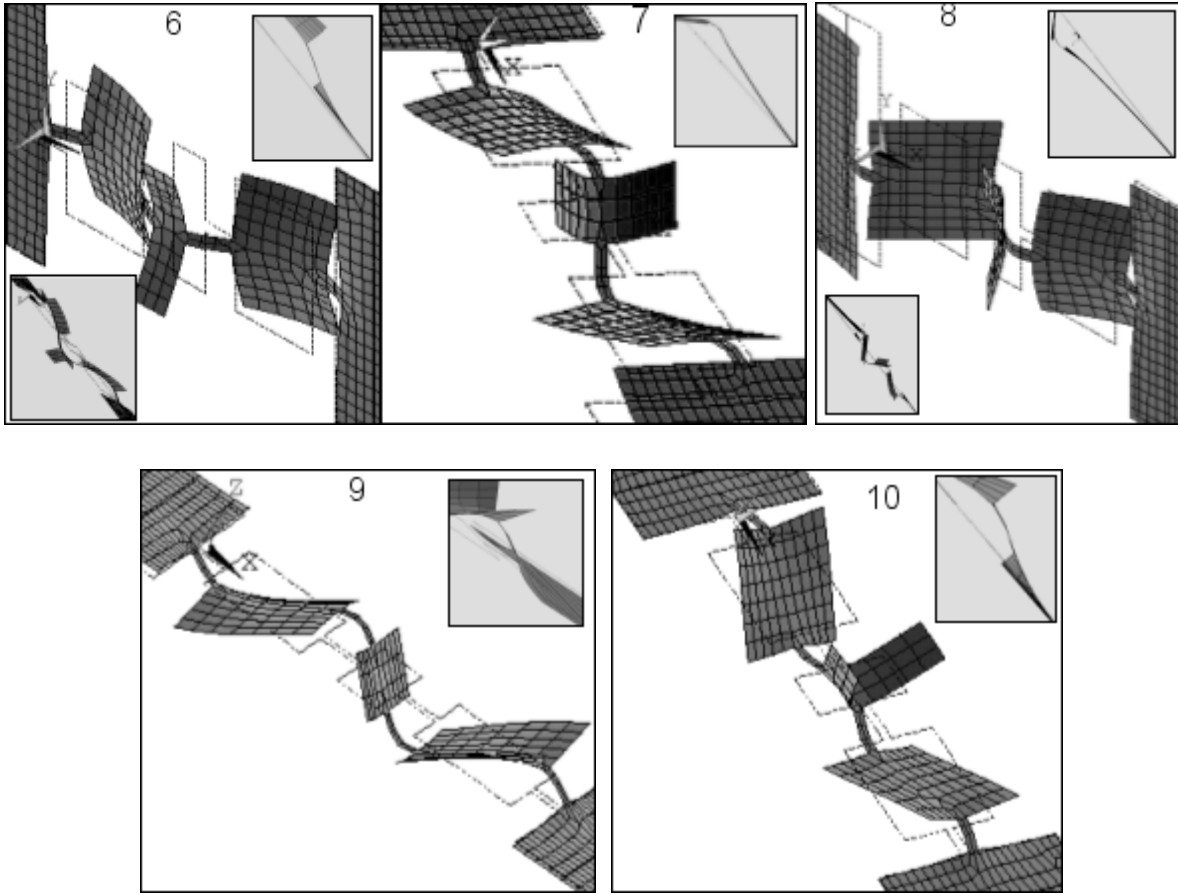


Figure 4. Modes six – ten of the triple torsional oscillator with the dimensions shown in Fig. 2. The upper right inset is a close-up view of where the wing is connected to the base via the neck. Lower insets, if applicable, are side-views of each mode given for ease of visualization.

of the region near the base is needed to estimate the ratio of the quality factors expected for each mode.

2.2. Experimental results

Characterization of the actual oscillators was done using a fiber optic interferometry system with a piezo-feedback circuit for fringe stability and a resolution of $0.002 \text{ nm/Hz}^{1/2}$.¹¹ The oscillators were attached to a piezoelectric material which was driven at the desired frequency. This shaking motion in turn excited the resonances in the oscillators, and amplitude of oscillation was detected with a lock-in amplifier.[†] Fig. 5 shows two typical frequency scans on two separate torsional oscillators from 5 – 90 kHz. The scans are performed in vacuum ($< 1 \text{ mTorr}$) to decrease the effects of substrate resonances. Clear resonances are observed in the same approximate range as was predicted by the finite element modeling. The observed resonance frequencies tended to be higher in magnitude, most likely due to the thickness being larger than the 200 nm used for modeling.

Phase-sensitive detection was employed in order to facilitate the assignment of the various modes. This was done by moving the laser spot to different locations on the oscillator and comparing the relative phases observed

[†]Because the method of excitation was purely a linear shaking movement, it is suspected that the torsional modes are not properly excited and therefore their amplitude is significantly reduced, if detected at all. The magnetic excitation method discussed in Section 3.2 should overcome this problem by applying the driving force only on one side of the oscillator.

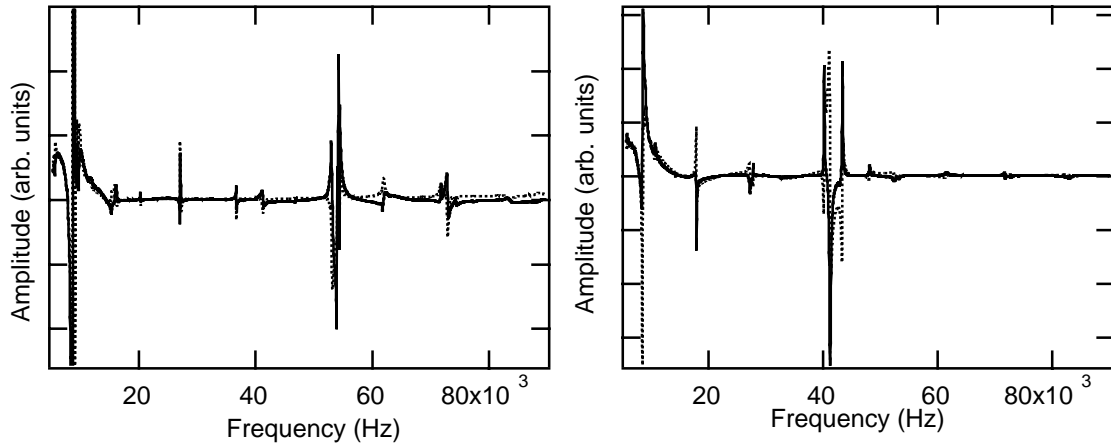


Figure 5. Typical frequency scans of triple-torsional oscillators. Solid line: x ; dotted line: y .

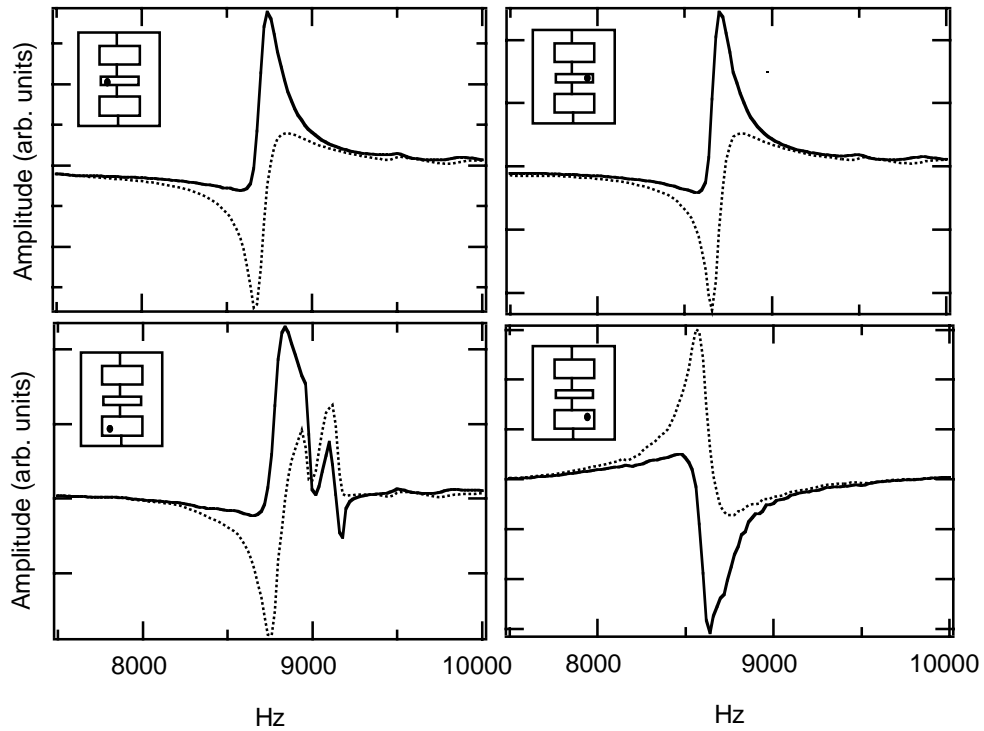


Figure 6. Phase-sensitive detection of the first bending mode of a triple-torsional oscillator, taken in four different locations as indicated by the upper left insets. Solid line: x ; dotted line: y .

at each spot. Fig. 6 shows the resonance results from four different locations on the same triple torsional oscillator. The phase-sensitive outputs x and y of the lock-in are plotted for each location. It can be seen that all four locations have the same phase, indicating that this is most likely the first bending mode. (The difference in the fourth plot is due to the fiber being on an adjacent interference fringe with an opposite slope, resulting in a signal with the same overall phase but opposite sign.) Fig. 7 shows a probable location for the upper torsional mode, in which the two sides of the head are of opposite phase, and no significant movement is detected for the

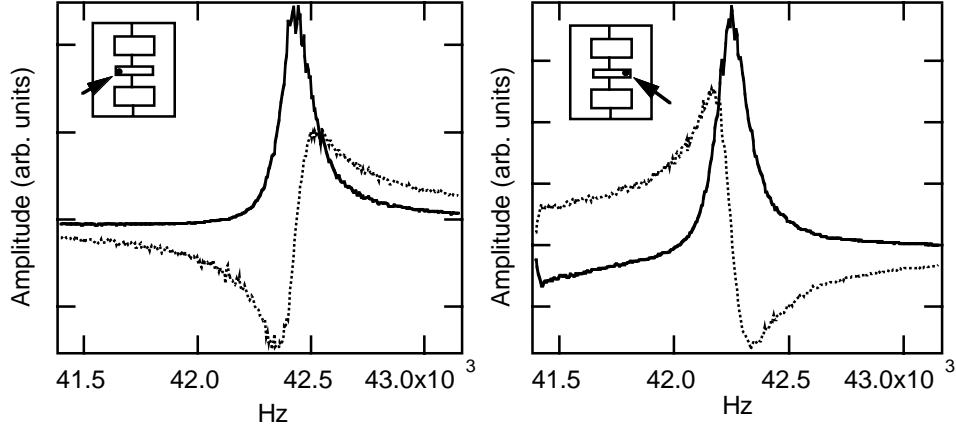


Figure 7. Phase-sensitive detection of the upper torsional mode of a triple-torsional oscillator, taken at opposite locations on the head as indicated by the upper left insets. Solid line: x ; dotted line: y .

wings. This resonance at approximately 42 kHz was the only one in the 5 – 90 kHz region which fit this criteria, and is therefore likely to be the desired upper torsional mode. However, due to the linear method of excitation, these results are tentative and new methods of excitation must be explored in order to fully characterize the torsional resonances. Capacitive excitation, as is done for large oscillators, is being considered, and Section 3.2 details the magnetic excitation method which is well underway.

Preliminary results from the other resonances tentatively support the mode predictions from finite element modeling. However, due to the slight asymmetry of the actual oscillator, many of the modes are split and overlap, causing phase sensitive detection to be difficult. Also, more locations on the oscillator need to be measured in order to identify the higher bending modes.

It has been shown that triple-torsional oscillators can be successfully fabricated with frequencies of the lowest modes are in the desired range for NMRFM (< 50 kHz). The details of this intended application are given in the following section.

3. APPLICATION TO NUCLEAR MAGNETIC RESONANCE FORCE MICROSCOPY

The previous section detailed the properties of the triple-torsional design which is intended for future use in a nuclear magnetic resonance force microscope. Due to the complexity of the field of NMRFM, initial experiments must first be performed before incorporating the triple-torsional design into the microscope. This section will discuss these initial experiments. First, the force detection of nuclear magnetic resonance has been successfully observed using a double-torsional micro-oscillator with an external permanent magnet. Also, magnets have been deposited onto oscillators in order to explore the possibility of magnetic excitation as well as the magnet-on-oscillator geometry of NMRFM.

3.1. NMRFM with a double-torsional micro-oscillator

Fig. 8(a) gives an overview of the set-up used in NMRFM. The magnetization in a sample is coupled directly to a mechanical oscillator through an applied field gradient. The magnetization is oscillated at the resonant frequency of the mechanical oscillator using rf radiation applied through a coil, and the resulting force is given by:

$$\vec{F} = (\vec{M} \cdot \vec{\nabla})\vec{B}. \quad (1)$$

The amplitude of oscillation is detected with a fiber optic interferometer, giving a measurement of the force and therefore the magnetization. The magnetization is inverted using a technique called cyclic adiabatic inversion,

in which the effective field in the rotating frame is oscillated about the axis of the coil at the resonant frequency of the oscillator. The magnetization follows this effective field, resulting in the force given by equation (1). Thus the resonant frequency of the mechanical oscillator must be low enough so that the effective field does not move too quickly and the magnetization will continue to follow it, leading to the 50 kHz upper limit discussed in the previous section.

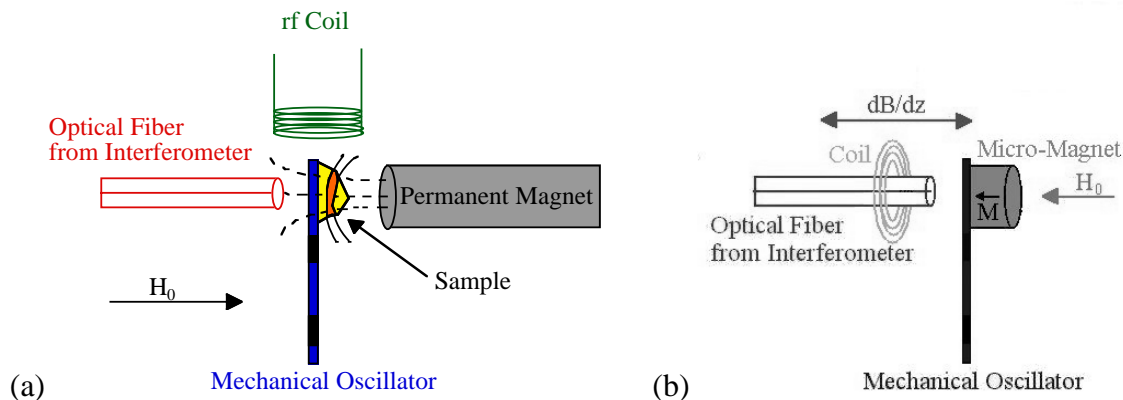


Figure 8. (a) Overview of the set-up used in magnetic resonance force microscopy. (b) Overview of the set-up used for magnetic excitation of mechanical oscillators.

The experiment discussed here was done in the sample-on-oscillator geometry. Samples were mounted manually onto the head of a double-torsional oscillator. Fig. 9(a) shows an SEM image of one such oscillator with a $5 \mu\text{m}$ sample on it. Once the sample has been mounted, the oscillator must be characterized to find its new resonant frequencies and Q 's, since the mass of the sample greatly decreases both of these. Fig. 9(b) shows the frequency scan of the oscillator used in the NMRFM experiment which had a $20 \mu\text{m}$ diameter sample of ammonium sulfate ($(\text{NH}_4)_2\text{SO}_4$) mounted to the edge of the head. Three main resonances are found below 10 kHz. The force sensitivity of each mode can be estimated from:

$$F_{min} = \sqrt{\frac{4k_B T k_{osc}}{Q\omega}}, \quad (2)$$

where Q and ω are determined from the frequency scans, and k_{osc} is the spring constant of the oscillator, estimated to be 0.01 N/m . The force sensitivities of the 850 Hz and the 5600 Hz resonances are both on the order of $5 \times 10^{-15} \text{ N/Hz}^{1/2}$. In order to estimate the force expected from the sample, the thickness of the resonant slice was estimated to be $8 \mu\text{m}$, (corresponding to an adiabatic inversion amplitude of 25 G and a field gradient of 300 T/m). Thus, a total of 1.7×10^{14} spins are estimated to be at resonance and therefore contributing to the observed signal. Taking into account the 8.073 T static field from the NMR magnet and a 0.35 T^\ddagger field from the permanent magnet, the Curie susceptibility of the nuclear magnetization yields a magnetic moment of $6.8 \times 10^{-17} \text{ J/T}$. Using this value with the 300 T/m field gradient gives the value for the force expected from the resonant slice: $F_{calc} \approx 2 \times 10^{-14} \text{ N/Hz}^{1/2}$. This value is approximately four times larger than the thermal noise of the oscillator and therefore sufficient for doing a single-sweep experiment.

The permanent magnet was initially placed 0.8 mm away from the oscillator with the intention of moving it further away in $10 \mu\text{m}$ steps. A location approximately 1.4 mm away from the oscillator was chosen as the target in order to account for variations in the estimated parameters. The cyclic adiabatic inversion began 400 kHz above resonance and decayed in less than 10 ms to the carrier frequency, which was set to $\frac{\gamma}{2\pi} H_{total} = (42.577 \text{ MHz/T})(8.073\text{T} + 0.35\text{T}) = 358.6 \text{ MHz}$. It then oscillated about this carrier frequency with an amplitude of 50 kHz and a frequency of 858.25 Hz .

[‡]All field and field gradient values have been calculated for the iron bar used: 24 mm long and 3 mm diameter.

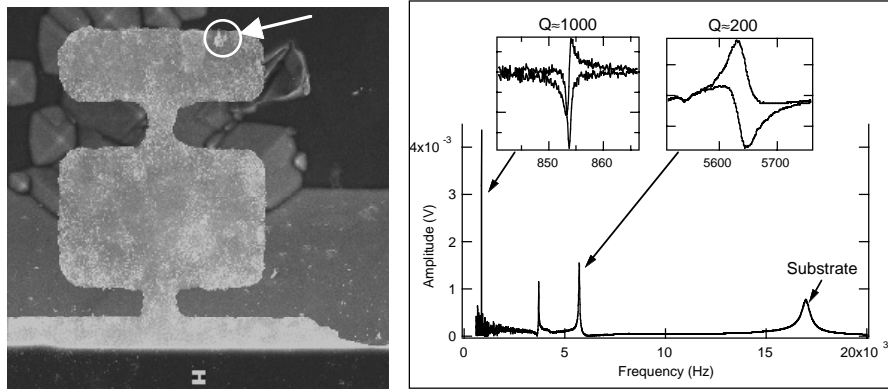


Figure 9. (a) SEM image of a double-torsional oscillator with a sample manually mounted onto it. (b) Frequency scan of the double-torsional oscillator used in the NMRFM experiment described in this work.

The position of the iron bar was moved in $10 \mu\text{m}$ steps from 0.8 mm to 1.9 mm. The solid circles in Fig. 10(a) shows the results of this position scan in the area of the sample. The amplitude of the measured signal at the end of each rf pulse is plotted for each position; no averaging was performed. From the data it is clear that there is a peak at 1.290 mm with a width of $20 \mu\text{m}$, approximately the same size as the sample.

To verify the NMR origin of this signal, the frequency was shifted up by 1 MHz to 359.6 MHz. This corresponds to $\approx 0.025 \text{ T}$, which in turn corresponds to roughly $100 \mu\text{m}$ in the region 1.3 mm away from the sample (as calculated from the magnetic field dependence as a function of distance). Therefore, it would be expected that this new frequency would result in the resonance moving approximately $100 \mu\text{m}$ towards the oscillator. The open squares in Fig. 10(a) indicate that this was indeed observed. The peak shifted towards the oscillator by $\approx 90 \mu\text{m}$, and the width was still $\approx 20 \mu\text{m}$.

To further investigate the observed signal, the magnet was held at the fixed position of 1.200 mm and the frequency was scanned. The results of this frequency sweep are given in Fig. 10(b), with a peak at 359.6 MHz as expected.

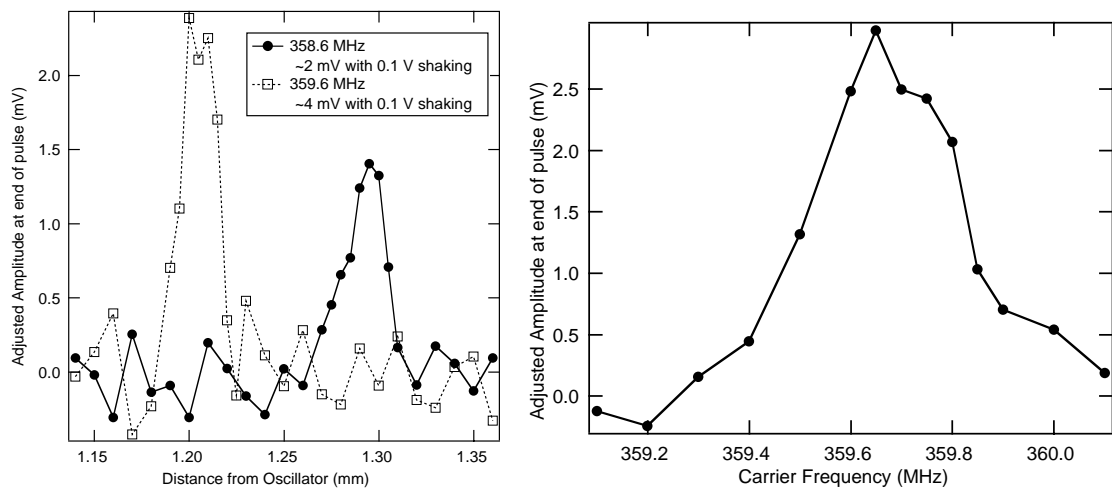


Figure 10. (a) Results of a position scan for a carrier frequency of: 358.6 MHz (solid circles), and 359.6 MHz (open squares). The slight change in amplitude is due to a lower quality of reflection for the 358.6 scan. (b) Results of a frequency scan at a fixed position 1.200 mm away from the sample.

The measured noise is on the order of a few tenths of a mV, as can be seen in Fig. 10(a), corresponding to a measured noise level of 3 angstroms. (An amplitude conversion of $1 \text{ mV} \approx 1 \text{ nm}$ has been used.) Using a Q of 1000 and a spring constant of 0.01 N/m , this translates to a noise level of $3 \times 10^{-15} \text{ N/Hz}^{1/2}$, in good agreement with the calculated value of $5 \times 10^{-15} \text{ N/Hz}^{1/2}$. The signal strength is on the order of 1.5 mV , corresponding to roughly 15 angstroms. This equals a measured force from the sample of $1.5 \times 10^{-14} \text{ N/Hz}^{1/2}$, in excellent agreement with the predicted value of $2 \times 10^{-14} \text{ N/Hz}^{1/2}$.

These results show the ability to use torsional micro-oscillators for the force detection of NMR, and efforts are underway to repeat this experiment with the triple-torsional designs discussed in this work.

3.2. Magnet-on-oscillator characterization

As mentioned previously, the experiment discussed here was done in the sample-on-oscillator geometry depicted in Fig. 8(a). However, the sample and magnet position can be switched without an effect on the resulting force. The magnet-on-oscillator configuration will allow for the high-Q characteristic of the torsional oscillators to be used without the large loss of sensitivity inherent in the sample-on-oscillator configuration.[§] In addition, mounting magnets onto the oscillators will allow for magnetic excitation as a means of characterizing the resonances, which will allow for better excitation of the torsional modes and more reliable phase-sensitive detection.

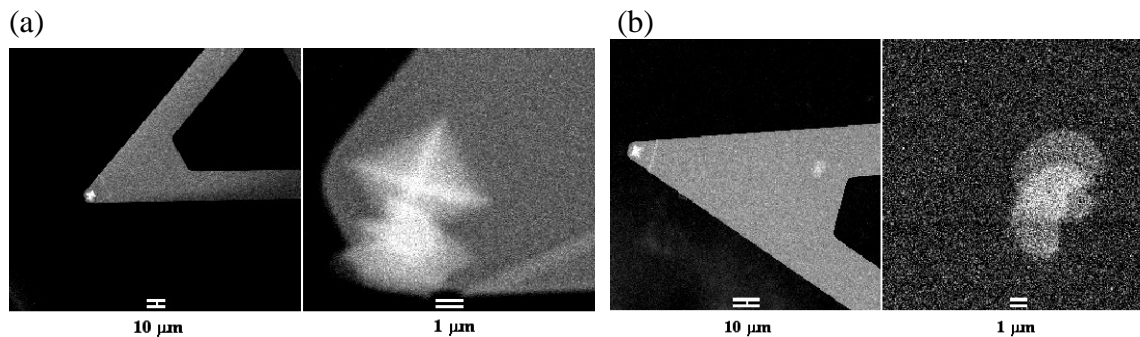


Figure 11. (a) SEM image of Ultralever cantilever with a magnet $4 \mu\text{m}$ in diameter, 60 nm cobalt capped with 8 nm gold. (b) SEM image of Ultralever cantilever with a magnet $2 \mu\text{m} \times 3 \mu\text{m}$, 83 nm cobalt capped with 12 nm gold. Only the bright center spot is considered for the magnet calculations; the surrounding regions of film are either gold with no underlying cobalt or cobalt that is exposed to air and, thus, oxidized.

An ultra-high vacuum (UHV) system equipped with two electron beam evaporators was used to deposit cobalt magnets capped with an anti-oxidation layer of gold. Cobalt layers were measured to be between $0.06 - 0.10 \mu\text{m}$. Availability of commercial cantilever-type oscillators and their characteristic data made these types of oscillators desirable for initial magnet-on-oscillator characterization. Micron-sized pinholes in stainless steel foil were used to shadow mask Park Scientific Ultralever AFM cantilevers.[¶] SEM images of two such cantilevers are shown in Fig. 11.

In order to measure the magnetic moment, a wire coil with radius 1.4 mm was placed 5 mm from the oscillator surface, with the optical fiber through its center (See Fig. 8(b)). The well defined field gradient of the coil interacts with the micro-magnet to produce a force on the oscillator. Typically, magnetic films of this thickness have an easy magnetic axis in the plane of the film. However, this shape anisotropy was overcome by applying

[§]Prior to sample mounting, the upper modes of the double-torsional oscillators have been found to have force sensitivities at room temperature as low as $1.5 \times 10^{-16} \text{ N/Hz}^{1/2}$.

[¶]It is important to note the interest in this study is in flat pancake geometry magnets for their well-understood field gradient. This is different from applications such as magnetic force microscopy (MFM) where a sharp magnetic tip is needed for high resolution. It is therefore desirable to deposit the magnet onto flat regions of the oscillator as close to the tip end as possible for the greatest induced force.

Micro- Magnet (Fig. #)	Calculated Cobalt Moment ($\frac{J}{T}$)	Expected Force (N)	Measured Force in air (N)
Ultralever (Fig. 11(a))	1.1×10^{-12}	8.6×10^{-14}	9×10^{-14}
Ultralever (Fig. 11(b))	7×10^{-13}	4.3×10^{-14}	3×10^{-14}

Table 2. Comparison of calculated and measured forces for micro-magnets on cantilevers.

a large static field of approximately 1 Tesla. The oscillator is driven by operating the coil with a sinusoidal current at the resonant frequency of the oscillator. The magnetic field gradient produced is approximately 10^{-2} T/m. Assuming the micro-magnet geometry is truly flat, one can calculate by volume the expected moment produced by the cobalt and compare with the force detected with the oscillator. Table 2 summarizes these comparisons. Reasonable agreement between the expected and measured forces has been found, indicating a successful demonstration of the magnetic excitation of micro-oscillators.

4. SUMMARY

Single-crystal silicon triple-torsional micro-oscillators have been fabricated for use in a nuclear magnetic resonance force microscope. Finite element modeling was done to determine the lowest ten modes. The connection to the base was considered in the model, and first observations indicate that the upper torsional mode significantly minimizes the damping due to losses to the fixed base. The modes were verified using a phase-sensitive fiber-optic interferometry system, and resonances were found in the desired range below 50 kHz. A demonstration sample-on-oscillator NMRFM experiment was performed using a double-torsional micro-oscillator. A single-sweep sensitivity of 3×10^{-15} N/Hz^{1/2} and a signal-to-noise ratio of 5 were observed at room temperature. The magnet-on-oscillator configuration has been explored both for use in NMRFM as well as magnetic excitation of torsional modes. Future work will focus on combining all the techniques discussed in this work in order to achieve a single-sweep sensitivity as low as 10^{-16} N/Hz^{1/2} at room temperature.

ACKNOWLEDGMENTS

This work was supported by the U. S. Army Research Office under contract DAAD-19-99C-0044, the Robert A. Welch Foundation under grant F-1191, the Texas Advanced Technology Program under grant 003658-0739-1999, and the National Science Foundation under grant DMR-0072365.

REFERENCES

1. J. A. Sidles, "Noninductive detection of single-proton magnetic resonance," *Appl. Phys. Lett.* **58** (1991) 2854 – 2856.
2. J. A. Sidles, "Folded Stern-Gerlach experiment as a means for detecting nuclear magnetic resonance in individual nuclei," *Phys. Rev. Lett.* **68** (1992) 1124 – 1127.
3. D. Rugar, O. Zugar, S. Hoen, C. S. Yannoni, H.-M. Vieth, and R. D. Kendrick, "Force detection of nuclear magnetic resonance," *Science* **264** (1994) 1560 – 1563.
4. O. Klein, V.V. Naletov, and H. Alloul, "Mechanical detection of nuclear spin relaxation in a micron-size crystal," *Eur. Phys. J. B* **17** (2000) 57 – 67.
5. Arnd Schaff and Wiebren S. Veeman, "Mechanically detected nuclear magnetic resonance at room temperature and normal pressure," *J. of Mag. Res.* **126** (1997) 200 – 206.
6. K. Wago, O. Zugar, R. Kendrick, C. S. Yannoni, and D. Rugar, "Low-temperature magnetic resonance force detection," *J. Vac. Sci. Technol. B* **14** (1996) 1197 – 1201.

7. O. Zugar, S. T. Hoen, C. S. Yannoni, and D. Rugar, "Three-dimensional imaging with a nuclear magnetic resonance force microscope," *J. Appl. Phys.* **79** (1996) 1881 – 1884.
8. T.A. Barrett, C. R. Miers, H. A. Sommer, K. Mochizuki, and J. T. Markert, "Design and construction of a sensitive nuclear magnetic resonance force microscope," *J. of Appl. Phys.* **83** (1998) 6235 – 6237.
9. Xiao Liu, S. F. Morse, J. F. Vignola, D. M. Photiadis, A. Sarkissian, M. H. Marcus, and B. H. Houston, "On the modes and loss mechanisms of a high Q mechanical oscillator," *Appl. Phys. Lett.* **78** (2001) 1346 – 1348.
10. C. L. Spiel, R. O. Pohl, and A. T. Zehnder, "Normal modes of a Si(100) double-paddle oscillator," *Rev. Sci. Instrum.* **72** (2001) 1482 – 1491.
11. M. D. Chabot and J. T. Markert, "Microfabrication of single-crystal silicon multiple torsional oscillators," *Proc. of the SPIE* **3875** (1999) 104 – 112.
12. H. Seidel, L. Csepregi, A. Heuberger, and H. Baumgartel, "Anisotropic etching of crystalline silicon in alkaline solutions: Orientation dependence and behavior of passivation layers," *J. Electrochem. Soc.* **137** (1990) 3612 – 3625.
13. H. Seidel, L. Csepregi, A. Heuberger, and H. Baumgartel, "Anisotropic etching of crystalline silicon in alkaline solutions: Influence of dopants," *J. Electrochem. Soc.* **137** (1990) 3626 – 3632.
14. G. Schropfer, S. Ballandras, M. de Labachellerie, P. Blind, and Y. Ansel, "Fabrication of a new highly-symmetrical, in-plane accelerometer structure by anisotropic etching of (100) silicon," *J. Micromech. Microeng.* **7** (1997) 71 – 78.
15. N. F. Raley, Y. Sugiyama, and T. Van Duzer, "(100) silicon etch-rate dependence on boron concentration in ethylenediamine-pyrocatechol-water solutions," *J. Electrochem. Soc.* **131** (1984) 161 – 171.
16. M. Elwenspoek, "The form of the etch rate minima in wet chemical anisotropic etching of silicon," *J. Micromech. Microeng.* **6** (1996) 405.